

ASSESSMENT OF GROUNDWATER RECHARGE POTENTIAL USING A STOCHASTIC ANALYTIC HIERARCHY PROCESS (SAHP)

Youssouf Koussoube ¹, Issan Ki ^{1,2}, Noura Dahri ³

¹Laboratoire Géosciences et Environnement, Unité de formation et de recherche en sciences de la vie et de la terre, Université Joseph KI-ZERBO, Ouagadougou P.O. Box 7021, Burkina Faso

²Unité de formation et de recherche en sciences Appliquées et technologies, Université Daniel OUEZZIN-COULIBALY, Dédougou, BP 139, Burkina Faso

³University of Sfax, BP 1171, 3000 Sfax, Tunisia

ABSTRACT

It is vital to map groundwater recharge potential if we are to manage water resources sustainably. This is particularly important in regions where hydrological stress is increasing. In this context, multi-criteria decision-making (MCDM) techniques that combine remote sensing and GIS have become valuable tools for spatial analysis and environmental assessment. Among these techniques, people use the Analytic Hierarchy Process (AHP) most widely. Saaty developed it in 1980. It has a structured approach to integrating multiple factors influencing recharge. However, the subjectivity involved in assigning criterion weights and defining class boundaries remains a major limitation, often leading to uncertainty in the resulting maps. To address this issue, the present study incorporates a Monte Carlo-based probabilistic approach into the AHP framework to quantify and reduce the influence of subjective judgments. This integration allows a more robust and objective evaluation of groundwater recharge potential by accounting for variability in expert opinions. Applied to the Niger Basin, the method demonstrates improved reliability in delineating areas with favourable recharge conditions, validated through piezometric data from observation wells. Overall, the AHP–Monte Carlo hybrid model enhances the credibility of recharge potential mapping by providing a more transparent and data-driven assessment of spatial uncertainty. These areas are located in the north and south of the basin, in the localities of Gorom Gorom, Dori, Bogandé, Gayérie and Diapaga. Furthermore, the AUC value of 0.757 recorded by the AHP model, compared to a slightly higher value of 0.763 recorded by the MC-AHP model, proves the superior performance of the latter.

KEYWORDS

Remote sensing and GIS, AHP method, Monte Carlo method, Recharge potential, Niger basin.

1. INTRODUCTION AND PROBLEMATICS

Multi-criteria decision-making models (MDMC) integrating remote sensing and GIS have attracted the attention of many researchers. Among them, hierarchical process analysis (AHP), first proposed by Saaty in 1980, is one of the most widely used MDMC approaches. It provides a rational framework for decision-making by compartmentalising issues into hierarchies, encompassing objective factors, criteria, and, should there be any, sub-criteria, in addition to decision alternatives [1]. The strength of the AHP lies in its ability to evaluate quantitative and qualitative criteria and alternatives on the same preference scale. Pairwise comparative judgements are given by decision-makers using numerical, verbal or graphical scales and are then synthesized to obtain overall priorities [2]. With regard to the mapping of aquifer recharge potential, the AHP model appears to give satisfactory results [3]. However, certain limitations have been observed in the implementation of this approach. The main difficulty lies in defining class boundaries and the weights assigned to the different criteria in the information system [4]. Most often, operators make the choice of class based on their ability to discern and their sense of judgement [5]. The outcome of recharge mapping can be significantly impacted by the selection of boundaries for class limits, as is the case with methods that rely on subjective evaluation [6]. A sensitivity study is required to establish the boundaries of the method and to ascertain the impact of the choice of class limits on the result. The incorporation of probabilistic Monte Carlo uncertainty into the AHP method is considered to be a powerful approach for quantifying the sensitivity and uncertainty of the proposed model. Indeed, the beta-PERT distribution has been widely used to model expert judgements and provides a close fit to normal distributions with little data [7, 8].

Groundwater contained in fissured and discontinuous aquifers is a relatively precious resource for Sahelian countries, given the early drying up of surface water. In Burkina Faso, for example, there were 58003 modern water points (wells and boreholes) in 2015 [9], making groundwater the main source of drinking water. However, the exploitation of groundwater often limited because of the complexity of identifying with a better precision, the dynamics in fissured and discontinuous aquifers [10].

The main objective of this research is to assess the sensitivity of the AHP model in mapping the recharge potential of aquifers in the Niger basin for better protection and availability of groundwater resources. The specific objectives consist, on the one hand, to provide valuable information on the recharge potential of aquifers and, on the other, to improve the quality and renewal of groundwater in the Niger basin of Burkina Faso.

2. CONTEXT OF THE STUDY AREA

The study area is the Niger watershed in Burkina Faso. It is located in the north-eastern part of the country. With a surface area of 58500 km², it is drained by the right bank tributaries of the River Niger (figure1B). The river Niger basin is shared by nine countries in West and Central Africa: Benin, Burkina Faso, Cameroon, Chad, Côte d'Ivoire, Guinea, Mali, Niger and Nigeria (figure1B). The Burkina Faso part of the basin, illustrated in Fig. 1C, is characterized by a flat topography that results in low surface water mobilization, which explains the very small number of hydro-agricultural structures and schemes [11]. Improved lowlands are not widespread, with around 660 ha [11]. There are fewer facilities for monitoring water resources, despite the abundance of natural underground resources (gold mines, gold panning sites, etc.). The 1:1 000 000 geological map [12] shows that the basin is underlain by Paleoproterozoic basement formations comprising paragneisses, basalts, sandstones (Tarkwaian type), gneisses, and volcanic rocks. This geological structure largely governs the characteristics of the groundwater systems,

which are hosted in discontinuous basement aquifers. Groundwater storage and flow only occur where the rock is fractured and/or weathered [13]. Altered zones are 10 to 80 m thick and represent the upper part of the basement aquifer[3]. The upper groundwater level can be between 5 and 30 m below the ground surface. Fractured basement aquifers can be between 10 and 80 m thick, and the level can be between 20 and 60 m below the ground surface[3]. A total of 1160 water points (wells and boreholes) have been identified in the basin area, based on the data available in the 2013 data sheet on modern water points produced by Burkina Faso's General Directorate for Water Resources (DGRE). These modern water points include improved wells and hand-pumped boreholes that provide valuable hydrogeological information, such as total depth, water level depth, duration of water availability before seasonal drying, and coping height. These water points are located in the communes of Gorom-Gorom, Djibo, Dori, Sebba, Bogandé, Boulsa, Gayeri, Diapaga and Fada N'Gourma (figure1C). Most of these are wells tapping the alterite aquifer, often situated near or along major river courses. The groundwater at this level is generally abundant and persistent, supporting small-scale vegetable gardening activities. However, in basement rock zones, groundwater exploration remains challenging, and numerous boreholes yield no water [11].

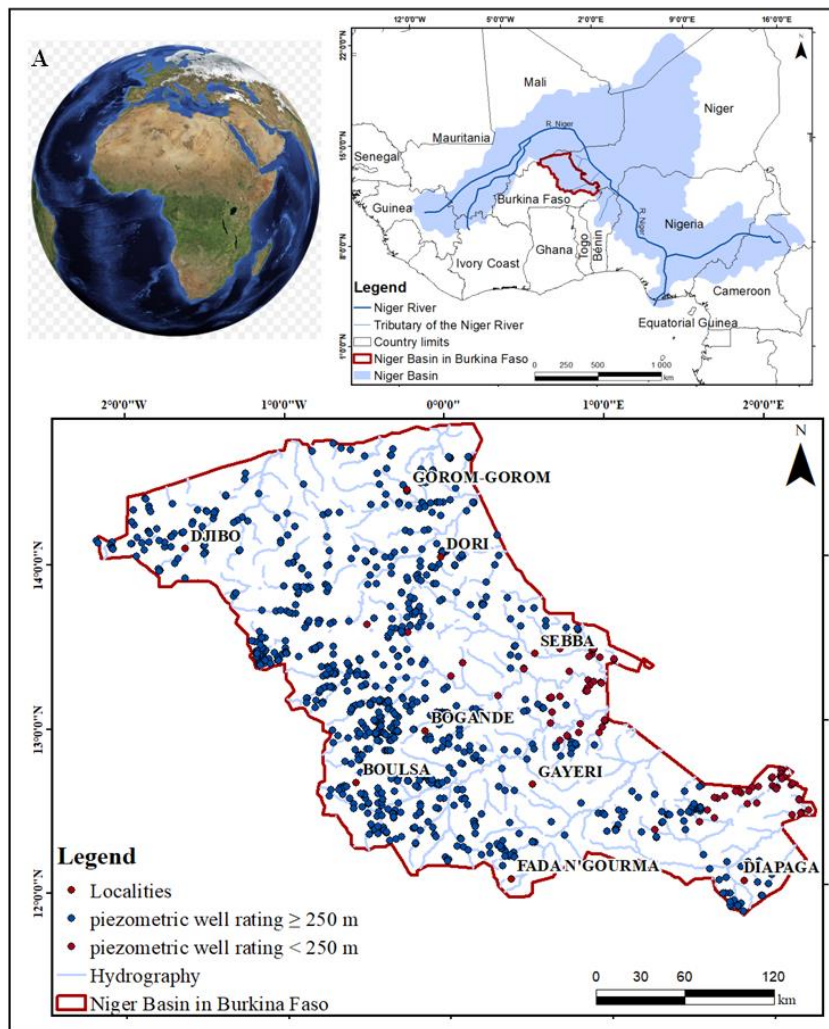


Figure1:Location map of the study area

3. MATERIALS AND METHODS

In this study, the main objective is to delineate potential groundwater recharge zones through the application of multi-criteria decision analysis (MCDA), specifically using the Analytic Hierarchy Process (AHP). To reduce subjectivity and account for uncertainty and sensitivity in the weighting process, the Monte Carlo simulation was integrated into the AHP framework, resulting in the MC-AHP approach, inspired by the works of [2], [3], and [6]. Multiple datasets from different sources were processed to derive the key criteria controlling aquifer recharge potential, including geology (lithology), soil type, hydrography (drainage density), fracture density (lineaments), slope, and land use/land cover [3, 4, 14, 15]. The choice of these criteria can be justified by their physical nature, which changes very little over time, unlike climatological criteria, which vary from year to year. They can also be easily mapped using remote sensing and GIS techniques.

Spatial analysis, classification, and overlay of these criteria were performed to generate a groundwater recharge potential map for the Niger Basin in Burkina Faso. Six (06) steps were essential in this process: (i) preparation and mapping of the thematic criteria layers; (ii) hydrodynamic classification and normalization of the criteria data; (iii) integration of Monte Carlo into the hierarchical analysis (MC-AHP); (iv) weighting of the criteria; (v) mapping of the recharge potential; (vi) validation of the recharge potential maps. The various stages of this work are illustrated in the conceptual diagram of the approach (figure 2).

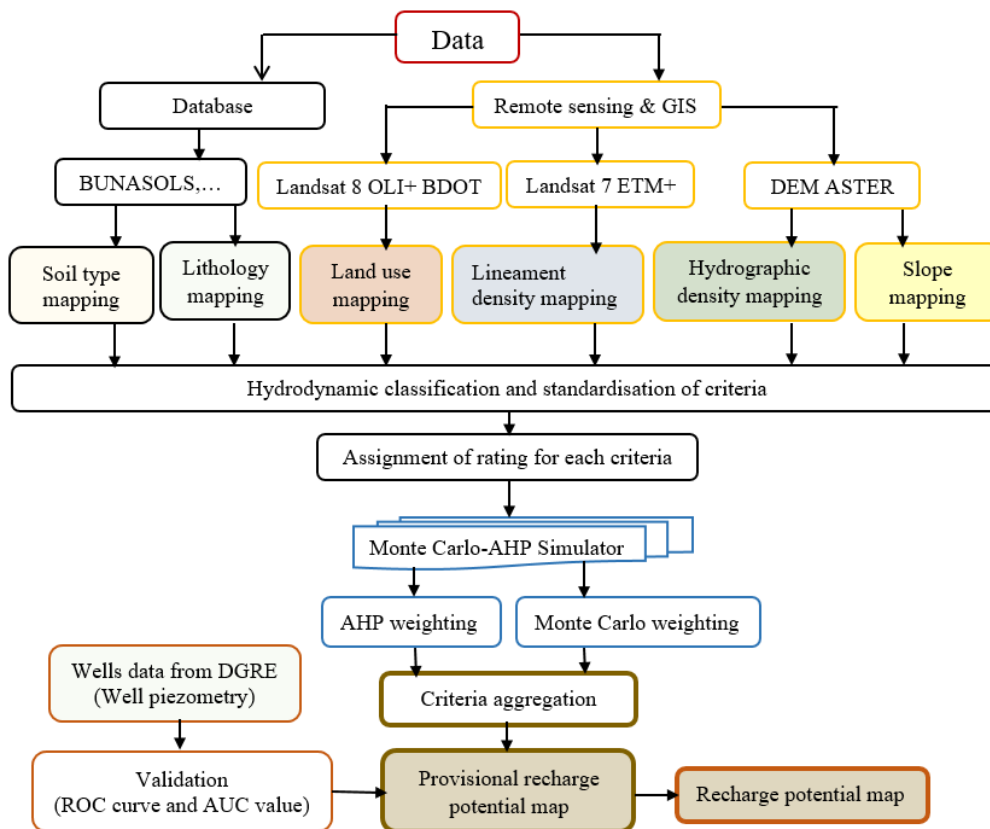


Figure 1: Methodology conceptual diagram

3.1 Data used

Several types of geospatial datasets were collected from various sources to support this study. A mosaic of Landsat 8 Operational Land Imager (OLI) images acquired in 2022 was downloaded from the USGS GLOVIS platform (<https://glovis.usgs.gov/>) to produce the land use map of the basin. These images, with a spatial resolution of 30 m, were selected based on their path–row coordinates covering the entire study area and were georeferenced in the UTM WGS 84 coordinate system (zone 30N).

Additionally, land use data (BDOT 2012) at a scale of 1:200,000, produced by the Institut Géographique du Burkina (IGB), were used to update and refine the 2022 land use classification. Geological data at a scale of 1:1,000,000 [12] were also obtained to delineate the lithological units of the study area.

The slope map of the basin was generated from the ASTER Digital Elevation Model (DEM), available via the USGS Earth Explorer platform (<https://earthexplorer.usgs.gov/>), which provides altimetry data with a 30 m spatial resolution. The hydrographic network was automatically extracted from the same DEM, and its drainage density was subsequently calculated.

To analyze lineament density, a Landsat 7 Enhanced Thematic Mapper Plus (ETM+) image an extract from a GeoCover mosaic acquired in October 2000 with a 30 m resolution was used. Soil type data were obtained from the *Bureau National des Sols* (BUNASOLS) of Burkina Faso, mapped at a scale of 1:1,000,000.

Finally, groundwater level data were collected from the 2013 modern water points database produced by the *Direction Générale des Ressources en Eau* (DGRE) of Burkina Faso, which provides valuable information for understanding the region's hydrogeological conditions.

3.2. Preparation of Criteria Thematic Maps

3.2.1. Lithology

The study area's lithological characteristics were derived from the geological map of Burkina Faso, which is available at a scale of 1:1 000 000 [12]. These data were used to delineate the main rock formations influencing groundwater occurrence.

3.2.2. Lineament density

Lineaments observed on satellite imagery generally correspond to fracture or fault zones, which serve as preferential pathways for groundwater flow. Their identification therefore provides valuable insight for hydrogeological exploration. The main methodological steps were as follows:

➤ *Pre-processing of Landsat 7 ETM+ imagery*

The initial stage involved radiometric correction to reduce image noise and geometric correction to ensure precise alignment with existing thematic layers such as geological, topographic, and photogeological maps [16]. The image was then orthorectified, achieving a pixel resolution of 14.5 m.

➤ *Processing of Landsat 7 ETM+ imagery*

Three spectral bands were selected Band 2 (green), Band 4 (near-infrared), and Band 7 (mid-infrared) to create a false-color composite (RGB 4-7-2) that enhances visual interpretation. Histogram equalization was applied to improve contrast and optimize information extraction. Further enhancement was achieved through the Hotelling transform, also known as Selective Principal Component Analysis (SPCA) [17–19], which reduces redundancy and highlights geological structures by producing new composite channels (neo-channels) derived from linear combinations of the original bands [20].

➤ *Manual extraction of lineaments*

Lineaments were manually digitized from the most representative neo-channel (ACP1) of the SPCA result. According to [18, 21], two approaches are generally applied for lineament extraction: manual digitization or filter-based enhancement. In this study, the manual method was used, supported by directional filters such as Laplacian and Sobel, to improve feature visibility at a 1:50,000 scale.

Fracture traces were identified based on morphological and tonal signatures, including linear vegetation alignments, abrupt lithological contacts, straight escarpments, and textural or tonal contrasts visible on the imagery.

➤ *Lineament density mapping*

The lineament density represents the total length of identified lineaments within a unit area of the catchment. To generate the density map, the study area was divided into regular grids of 3×3 km². Within each grid, the cumulative lineament length was calculated, and the results were interpolated to produce a continuous density surface across the basin.

3.2.3. Density of the hydrographic network

The drainage network was extracted automatically using DEM ASTER. The drainage density is the total length of the hydrographic network per unit area of the catchment considered. To determine this, the hydrographic network in the study area was discretized into regular grids of 3×3 km². In each mesh, the cumulative length of the drains was determined. By interpolating the cumulative length of the drains per mesh, the drainage density map per watershed can be generated.

3.2.4. Land use

The land cover classification of the study basin was derived from Landsat 8 Operational Land Imager (OLI) imagery acquired in 2022. A false-colour composite was created using spectral bands 5, 4, and 3, which correspond respectively to the near-infrared (NIR), red, and green portions of the electromagnetic spectrum. This band combination is commonly applied in remote sensing studies to enhance the discrimination between vegetated and non-vegetated surfaces and to reveal features that are not perceptible in true-colour imagery [22]. Subsequently, supervised classification techniques were employed to generate an updated land cover map. Training samples representing the principal land use classes were selected using the BDOT 2012 dataset, produced by the Institut Géographique du Burkina (IGB) at a 1:200,000 scale. This ancillary dataset facilitated accurate delineation of land cover categories and improved classification reliability for the 2022 map.

3.2.5. Slope

The slope map of the basin was derived from the ASTER Digital Elevation Model (DEM), which provides 30 m spatial resolution elevation data. The slope layer was used to characterize surface runoff dynamics and to evaluate areas favorable for groundwater infiltration and recharge.

4.1.6. Soil types

Information on soil distribution across the study area was obtained from the Bureau National des Sols (BUNASOLS) database of Burkina Faso. The dataset, available at a 1:1,000,000 scale, was used to identify and classify soil types influencing infiltration capacity and recharge potential.

3.3. Hydrodynamic classification and data standardization

The various criteria, which were originally expressed in different units and measured at different spatial scales, were made comparable by applying hydrodynamic classification and data normalisation. The hydrodynamic classification was carried out according to the hydrogeological properties of each parameter, particularly their infiltration capacity, which plays a key role in groundwater recharge processes [3]. To facilitate the multi-criteria analysis, the number of hydrodynamic classes was limited to five categories, following the classification schemes proposed in [23] and [24]. These classes are defined as low, moderate, average, good, and excellent. Subsequently, a standardized rating scale ranging from 1 to 10 was assigned to each class, in accordance with approaches commonly adopted in similar studies [4, 14, 23, 24] (Table 1).

Table 1: Standardized assessment scale

Hydrodynamic class	Low	Moderate	Average	good	Excellent
Standardisation of classes	1	3	5	7	10

3.4. Weighting of criteria

3.4.1. AHP comparison matrix

The Analytic Hierarchy Process (AHP) is widely applied for addressing complex decision-making problems, particularly those requiring pairwise comparisons between criteria [25]. This approach relies on a mathematical framework in which weighting coefficients are assigned to each criterion, ensuring that their total sum equals one [26]. To determine the relative importance of the criteria, an expert-based pairwise comparison matrix must first be constructed. This matrix, denoted as A , is a square matrix of size $K \times K$, where K corresponds to the number of evaluation criteria. Each element a_{ij} of the matrix represents the relative importance of criterion i compared to criterion j . The general form of this comparison matrix is presented in Equation (1).

$$A = \begin{bmatrix} 1 & a_{12} & \cdot & \cdot & \cdot & a_{1K} \\ 1/a_{12} & 1 & \cdot & \cdot & \cdot & a_{2K} \\ \cdot & \cdot & 1 & \cdot & \cdot & \cdot \\ \cdot & \cdot & \cdot & 1 & \cdot & \cdot \\ \cdot & \cdot & \cdot & \cdot & 1 & \cdot \\ 1/a_{1K} & 1/a_{2K} & \cdot & \cdot & \cdot & 1 \end{bmatrix} \quad (1)$$

In this study, eight matrices were developed by pairwise comparative judgements of the criteria given by the experts using the standardized evaluation scale (Table 1).

3.4.2. Weighting by the AHP model

The development of the AHP model involves several sequential steps:

Step 1: For each non-diagonal element of the pairwise comparison matrices, expert judgments are combined to generate a corresponding beta-PERT distribution using the three-point estimation approach [27]. This approach models uncertainty in expert evaluations through a beta-PERT distribution, which requires only three parameters minimum, most likely (mode), and maximum values making it particularly suitable for decision-making contexts.

Step 2: Identify the minimum (min), most likely (mode), and maximum (max) values for each non-diagonal element. For instance, if expert assessments for a_{13} (see Equation 1) are 1, 2, 1, 4, 3, 5, 4, and 3, then the respective values of min, mode, and max for a_{13} are 1, 3, and 5.

Step 3: Apply the PERT formula to calculate the mean (avg) and standard deviation (sd) of the non-diagonal elements, as defined in Equations (2) and (3).

$$avg = \frac{min + 4mod + max}{p} \quad (2)$$

$$sd = \frac{max - min}{p} \quad (3)$$

Where p is the number of experts

Step 4: Calculate the α and β coefficients from the corresponding beta-PERT distributions (equations 4 and 5).

$$\alpha = \left(\frac{avg - min}{max - min} \right) \left(\frac{(avg - min)(max - avg)}{sd} - 1 \right) \quad (4)$$

$$\beta = \left(\frac{max - avg}{avg - min} \right) \alpha \quad (5)$$

Step 4: Stochastically produce the beta-PERT distributions and generate the elements of the new matrix A_n as defined in equation 6.

$$a_{ij} = min + beta(\alpha, \beta)(max - min) \quad (6)$$

The 'weight' vector W of the new matrix A_n is calculated by aggregation. The eigenvector of this matrix is one of the best solutions used to determine the overall valuation of each action. By solving equation 7, the maximum eigenvalue λ_{max} and the eigenvector W are calculated [28].

$$A_n \cdot W = \lambda_{max} W \quad (7)$$

The value λ_{max} is always greater than the rank of the matrix (n). For a matrix close to the coherence condition, λ_{max} is close to (n). A coherence index CI was therefore defined (equation 8) to measure the degree of coherence of the matrix by calculating the product of the comparison matrix by the weight vector W and summing the elements of the resulting vector.

$$CI = \frac{(\lambda_{max} - n)}{(n - 1)} \quad (8)$$

The consistency ratio (CR) of the matrix is defined by equation 9, which compares CI to a random index (RI) generated independently of the sample size [1]. The CR must not exceed 10% for consistency to be acceptable.

$$CR = \frac{CI}{RI} \quad (9)$$

3.4.3. Weighting by the Monte Carlo AHP model

The Monte Carlo method uses the most likely (mode), minimum and maximum values of the expert estimates to generate a probability distribution that measures the level of confidence in the AHP decision [29]. The same AHP steps and constraints are used with the introduction of beta randomness (beta-rnd function). The beta-rnd is a function under MATLAB that generates beta distributed numbers in the interval of [0, 1] using form factors α and β [6]. Equation 6 used in the AHP method is replaced by Equation 10.

$$Random = min + betarnd(\alpha, \beta)(max - min) \quad (10)$$

The random numbers that follow the beta-PERT distributions are generated stochastically for the non-diagonal elements of each pairwise comparison matrix using the MATLAB random number generator with a certain number of replications (from 100 to 10 000).

3.5. Map of recharge potential

The generation of the recharge potential map involves spatially integrating the computed values of the recharge index (R). This process requires combining the normalized scores of the various criteria with their corresponding normalized weights, represented by the eigenvector components (w_i) of each criterion (see Equation 11). The recharge index is thus obtained by summing the products of the normalized ratings (X_i) and their respective weights (w_i):

$$R = \sum_{i=1}^K X_i w_i \quad (11)$$

Where X_i is the overall score for criterion i and w_i is the weight for criterion i .

3.6. Model validation

Piezometry is an effective tool for validating groundwater recharge potential in unsaturated zones. It was selected for this study because it provides a direct measure of aquifer recharge. Several authors in West Africa have applied this approach to evaluate the recharge potential of aquifers [30–34]. The method is particularly effective when the temporal scale is short enough to capture a full recharge-discharge cycle [30, 35]. In addition, piezometric analysis is relatively simple to apply, as it requires only limited data specifically, groundwater level measurements. The piezometric head is obtained by subtracting the groundwater level and the height of the well's curbstone from the ground elevation. In this study, water table levels were derived from the 2013 inventory of modern water points produced by the *Direction Générale des Ressources en Eau* (DGRE) of Burkina Faso. A total of 1160 water points were analyzed to validate the models. The piezometric data were divided into two categories (figure 1C). A threshold value of 250 m was adopted to identify recharge zones within the basin. This value was determined based on local piezometric conditions: areas with piezometric levels below 250 m were considered to have low recharge potential. Receiver Operating Characteristic (ROC) curves were then generated for the recharge models (AHP and MC-AHP) using the piezometric level dataset, where piezometric

levels ≥ 250 m were treated as true positives and levels < 250 m as false positives. The ROC curve is a widely used tool for evaluating classifier performance, as it examines the relationship between true and false positive rates [25, 36, 37]. The ROC curve represents a probability distribution, while the *Area Under the Curve* (AUC) quantifies the degree of separation between different groups [38]. Model accuracy is measured on a scale from 0 to 1, with higher values indicating higher model accuracy [39]. According to [40], AUC values of 0.5–0.6, 0.6–0.7, 0.7–0.8, 0.8–0.9, and 0.9–1 correspond respectively to low, moderate, good, very good, and excellent model performance.

4. RESULTS AND DISCUSSION

4.1. Recharge criteriamapping

Groundwater recharge potential in the study basin is governed by a combination of geological, structural, topographic, pedological, and land use factors that together control the infiltration, percolation, and storage of water within the subsurface. Among these, lithology plays a fundamental role, as it determines the capacity of geological formations to retain and transmit water. Under comparable environmental conditions, certain rock types such as porphyroid granite, pre- or syntectonic granite, migmatite, and veins provide more favorable conditions for groundwater flow than others, including post-tectonic granite, schists, and greenstone. Fracturing and metamorphic deformation further enhance the permeability of these formations, increasing their ability to store and convey water. Geological data at a scale of 1:1000000 for Burkina Faso [12] indicate that most of the study area is composed of Paleoproterozoic gneissic formations (Gn) intersected by basalts (Bs), felsic to intermediate intrusions, felsic volcanics (Vf), Tarkwaian conglomeratic quartzite and siltstone sandstones (Gr), and paragneisses (Pgn) (figure 3A). The extensive occurrence of these metamorphic formations, combined with the region's arid climate, contributes to the generally unsaturated state of local aquifers [41].

The structural context, represented by the density of lineaments, is also a key determinant of recharge potential. Lineaments correspond to fractures and faults that increase secondary porosity and create preferential pathways for groundwater infiltration and flow [42]. In basement terrains, aquifers are discontinuous, and recharge is mainly localized along fracture zones, veins, and lithological contacts where effective rainfall can percolate downward. Analysis of Landsat 7 ETM+ imagery revealed high to moderate lineament densities in the southern part of the basin, corresponding to a major NW–NE deformation corridor, and a smaller deformation zone in the north. The calculated lineament density values range from 0 to 0.6 km^{-1} and were classified into five categories (figure 3B). Areas with high lineament density are therefore considered more favorable for aquifer recharge due to the presence of enhanced permeability zones.

Closely linked to these structural and geological characteristics, drainage density reflects the balance between surface runoff and infiltration. It depends primarily on the underlying lithology, the degree of fracturing, and local topography. Low drainage density indicates permeable formations that favor infiltration, whereas high drainage density generally corresponds to impermeable rocks or steep slopes where runoff dominates. Using ASTER DEM data, drainage density in the basin was estimated to vary between 0 and 0.18 km^{-1} and was grouped into five classes (figure 3C). The highest values occur in the northern and central parts of the basin, corresponding to areas of high runoff and limited infiltration, while lower drainage densities are associated with zones more conducive to recharge.

Topography, expressed by slope gradients, also exerts a direct influence on recharge dynamics by controlling the partitioning of rainfall between infiltration and runoff. Gentle slopes promote

infiltration and groundwater recharge by reducing runoff velocity, whereas steep slopes favor surface drainage and limit the time available for infiltration. In the study area, slope values range from 0 to 12.10% and were classified into five categories (figure 3D). The flattest zones, characterized by minimal slopes, represent the most favorable environments for effective recharge.

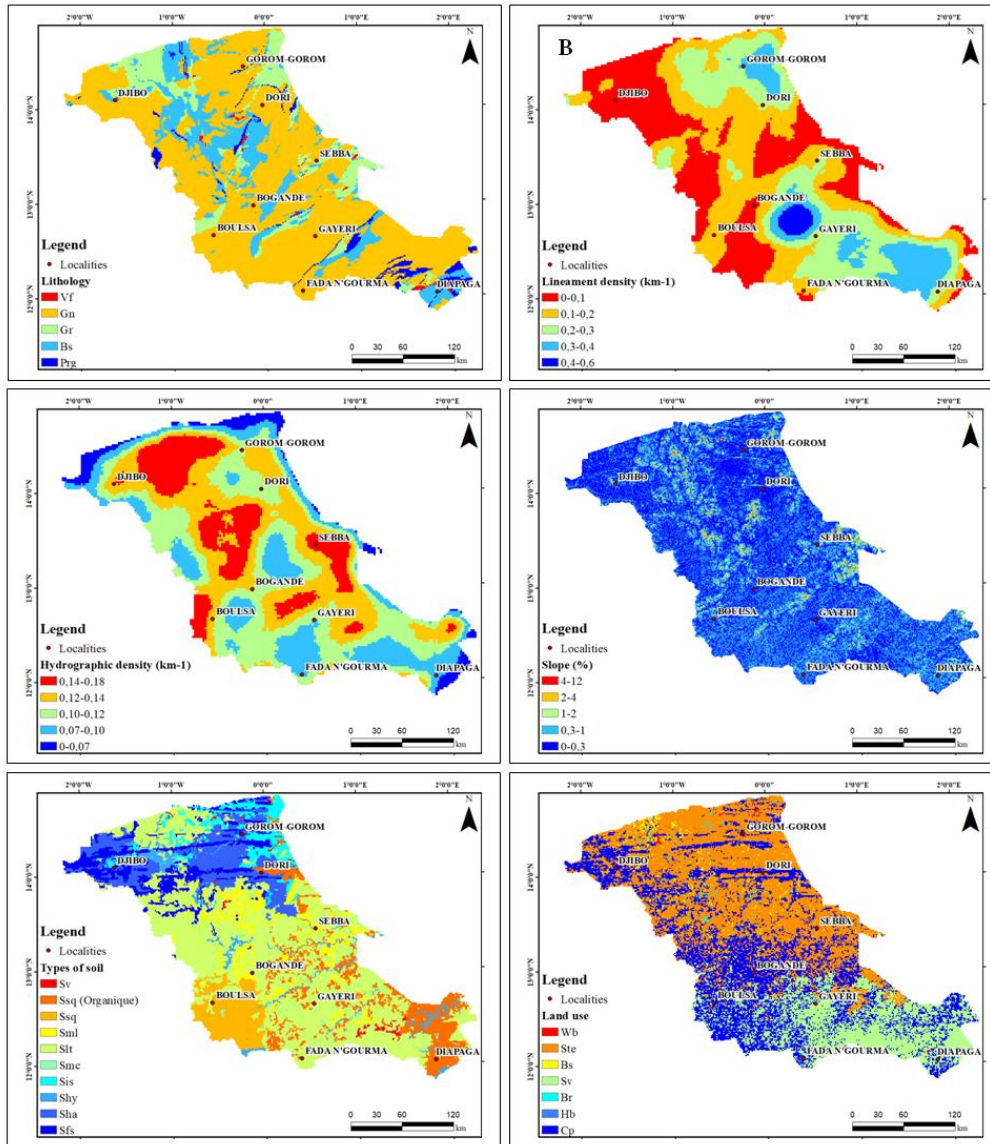


Figure 3:A) Lithology map; B) Lineament density map; C) Hydrographic network density map; D) Slope map; E) Soil type map; F) Land use map

The nature of soils further conditions the infiltration capacity and water retention properties of the surface layer. Soil data provided by BUNASOLS reveal ten soil types within the basin, including fersiallitic (Sfs), halomorphic (Sha), hydromorphic (Shy), isohumic (Sis), crude mineral (Smc), weakly developed (Slt), mull (Sml), sesquioxide (Ssq), and vertisols (figure 3E). These soils were reclassified according to the national study by [13], based on their readily usable water reserve (RFU). Soils with higher RFU values such as hydromorphic and fersiallitic soils tend to enhance infiltration and recharge, whereas those with low RFU favor surface runoff [43].

Finally, land use and land cover (LULC) significantly influence recharge potential by modifying infiltration rates and surface water dynamics. Vegetated areas, such as savannahs and forests, tend to increase infiltration and reduce runoff, while bare or urbanized surfaces promote rapid surface flow. The classification of Landsat 8 OLI images (bands 5, 4, and 3, 2022) identified seven land use categories: bare rock (Br), water bodies (Wb), settlements (Hb), bare soil (Bs), savannah (Sv), cropland (Cp), and steppes (Ste) (figure 3F). The basin is predominantly covered by steppes, savannahs, and cultivated areas, which together create favorable conditions for groundwater recharge by facilitating infiltration and reducing surface runoff.

Taken together, these six criteria including lithology, lineament density, drainage density, slope, soil type, and land use interact closely to define the spatial variability of recharge potential. Areas characterized by permeable lithologies, dense fracturing, gentle slopes, permeable soils, and vegetated land cover are expected to exhibit higher groundwater recharge capacity, whereas regions dominated by impermeable rocks, steep slopes, and sparse vegetation tend to experience limited infiltration and lower recharge potential. The hydrodynamic evaluations of the data for each criterion (infiltration capacity) enabled all the data for each criterion to be standardized from 1 to 10 according to their degree of involvement in aquifer recharge. This assessment is based on a literature review of several studies on the factors governing recharge (Table 2).

Table 2: Normalisation of criteria data

Criteria	Standardisation of recharge criteria data				
	1	3	5	7	10
	Low	moderate	Average	Good	Excellent
LT	Vf	Gn	Gr	Bs	Pgn
DL (km ⁻¹)	0-0,1	0,1-0,2	0,2-0,3	0,3-0,4	0,4-0,6
DH (km ⁻¹)	0-0,07	0,07-0,10	0,10-0,12	0,12-0,14	0,14-0,18
OT	Br, Wb	Hb	Bs	Sv	Cp, Ste
PT (%)	4-12	2-4	1-2	0,3-1	0-0,3
TS	Sfs, Ssq, Sml	Shy	Smc	Slt	Sis, Sv, Sha

Notes: land use (OT); lineament density (DL); drainage network density (DH); slope (PT); soil type (TS); lithology (LT).

4.2. Weighting of criteria

To address the lack of information and variations in expert judgment, a PERT-based normal distribution using Monte Carlo simulation was integrated into the AHP method to determine the criteria weights. All pairwise comparison matrices provided by the eight experts satisfied the consistency requirement ($CR < 10\%$). The relative weights of the criteria for each method were calculated with a 95% confidence level (Table 3).

It can be seen that the weights of land cover, lineament density, drainage network density, slope, soil type and lithology generated by AHP and MC-AHP are not of the same order of magnitude. It is important to note that for all the MC-AHP simulations, the coherence ratio was less than 0.1.

In the stochastic model, the weights of land use, lineament density, hydrographic network density, and soil type increased, whereas slope and lithology exhibited the opposite trend. Within this case study, slope and lithology can therefore be considered the least sensitive criteria in assessing groundwater recharge potential using the AHP approach. The probability density distributions of the criteria weights, obtained through the kernel-smoothing method, further support these findings by displaying lower probability densities for lithology (1.3×10^{-3}) and slope (1.7×10^{-3}).

Conversely, soil type exhibits the highest probability density, indicating that, irrespective of expert judgment, this criterion exerts the greatest influence on aquifer recharge potential. High recharge potential zones are also strongly associated with areas of dense hydrographic networks and lineament concentrations, particularly when these two factors coincide. Slope and land use make comparable contributions to recharge potential, while lithology remains the least influential factor.

Table 3: Weightings of the various criteria generated by AHP and MC-AHP

Criteria	AHP	MC-AHP	Standard deviation MC-AHP	95% confidence interval (MC-AHP)
OT	0,1742	0,226	0,0197-0,0203	0,2256-0,2263
DL	0,2456	0,3208	0,0229-0,0236	0,3203-0,3212
DH	0,0445	0,1197	0,0112-0,0115	0,1195-0,1199
PT	0,2487	0,1857	0,0254-0,0261	0,1852-0,1862
TS	0,0443	0,0579	0,0053-0,0054	0,0578-0,0580
LT	0,2427	0,09	0,0233-0,0240	0,0895-0,0905

Notes: land use (OT); density of lineaments (DL); density of hydrographic network (DH); slope (PT); soil type (TS); lithology (LT)

4.3. Spatial modelling of AHP and stochastic AHP recharge

The recharge potential indices AHP and stochastic AHP calculated using equation 8 were spatialized at the basin scale (figure 4 and 5). The number of recharge classes was reduced to five (05), as in other studies [23, 24], in order to facilitate interpretation of the results. Overall, the zonation of recharge potential ranges is similar between the two options (AHP model and stochastic AHP model). However, the integration of the Monte Carlo simulator (stochastic approach) has made the AHP model more flexible. Indeed, the Monte Carlo simulator indicates an extension of the zones where the recharge potential is favorable or very favorable. The reason for this increase is that the limits of the recharge potential classes operated by the experts have been adjusted, with a view to bringing them closer to reality on the ground. Correlatively, there is a reduction in unfavorable or very unfavorable recharge areas. Therefore, in the context of discontinuous aquifers, slight modifications can have an impact on the distribution of recharge zones.

Favorable recharge potential zones can be identified in the northern (Gorom Gorom, Dori) and southern (Bogandé, Gayérie and Diapaga) localities. There are a few pockets to the north and south of Djibo. The areas with moderate recharge potential are located in Djibo, Boulsa and Sebba. Similarly, unfavorable or even very unfavorable areas in terms of recharge potential are found mainly in these latter localities.

The ROC and AUC results for the two-aquifer recharge potential models in the Niger Basin, Burkina Faso, are presented in figure 6. The area under the ROC curve (AUC) provides an overall measure of model performance, while the ROC curve itself offers a clearer understanding of how model accuracy varies with changes in true and false positive rates [11].

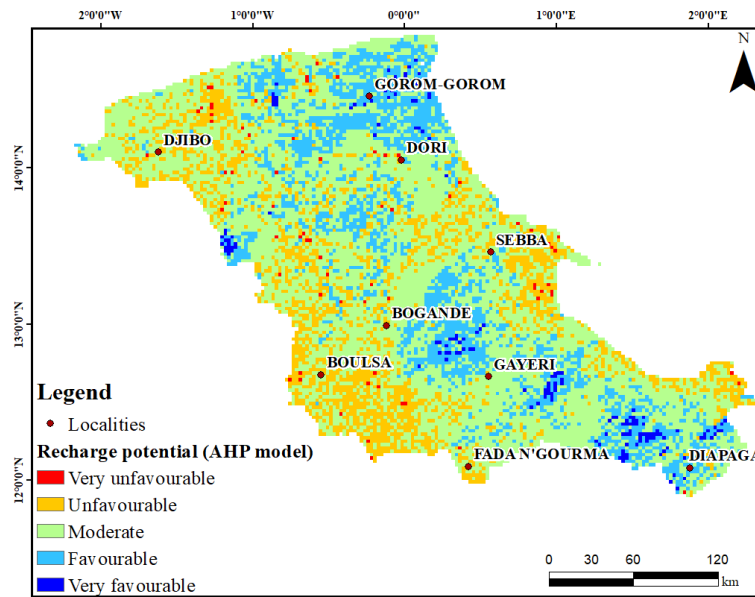


Figure 2: Recharge potential according to the AHP mode in the Niger basin

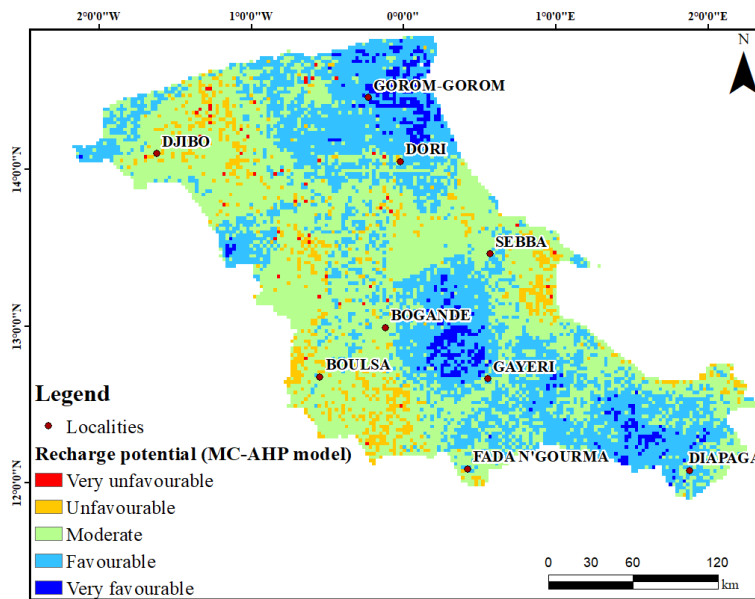


Figure3: Recharge potential according to the MC-AHP model in the Niger basin

Considering the AUC values (ranging between 0.7 and 0.8), both models demonstrate satisfactory predictive accuracy. However, the AHP model recorded an AUC value of 0.757, whereas the MC-AHP model achieved a slightly higher value of 0.763, indicating its superior performance. Furthermore, the ROC curve of the AHP model initially appears irregular between 0.2 and 0.4, reflecting an imbalance between true and false positive classifications. In contrast, the ROC curve of the MC-AHP model displays a smoother and more consistent alignment with the reference line, suggesting improved classification accuracy. These findings confirm that incorporating Monte Carlo simulation into the AHP framework enhances the representation of expert judgment, resulting in a model that better reflects actual field conditions.

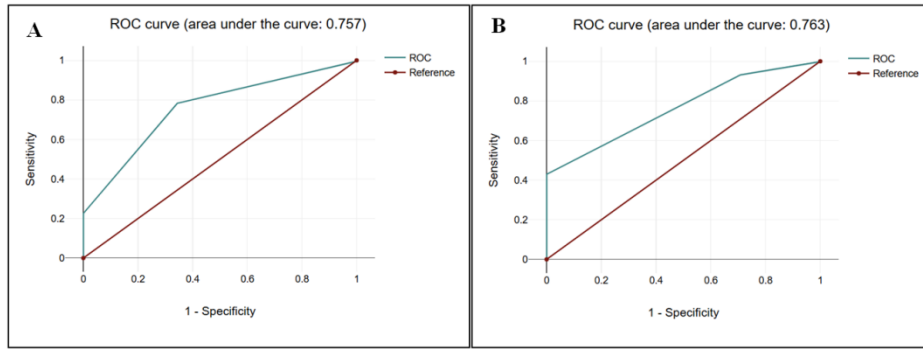


Figure 6: ROC curve for validation of aquifer recharge potential in the Niger basin: A) AHP model; B) MC-AHP model

Regarding recharge and groundwater potential zones, as part of the Water Supply and Sanitation Programme (PAEA) [13], the CACI/SERAT consortium developed a hydrogeological potential map of the Niger Basin in Burkina Faso. This map highlights highly productive zones distributed across the southern part of the basin, particularly around Bogandé, Gayéri, Fada N’Gourma, and Diapaga, where groundwater yields exceed 5 m³/h (figure 7). On the other hand, hydrogeological potential is predominantly unfavorable or moderate in the localities to the north of the basin (Gorom Gorom and Dori). By comparing these hydrogeological potentials with recharge potentials (MC-AHP modelling), it is possible to analyze water flows in the hydrosystem (the relationship between rainwater and groundwater) of the Niger basin in Burkina Faso. The unfavorable or moderate hydrogeological potential in the localities of Gorom Gorom and Dori can be explained by the fact that these localities are located in areas of very favorable recharge by rainwater, as shown on the recharge potential map (figure 5). This would encourage groundwater to flow southwards towards Bogandé, Gayéri, Fada N’Gourma and Diapaga, thereby increasing the productivity of the aquifers in these localities. It is therefore essential to pay particular attention to Gorom Gorom. The same is true of Dori. This is because they are key to improving the quality and renewal of the water tables in the Niger watershed in Burkina Faso.

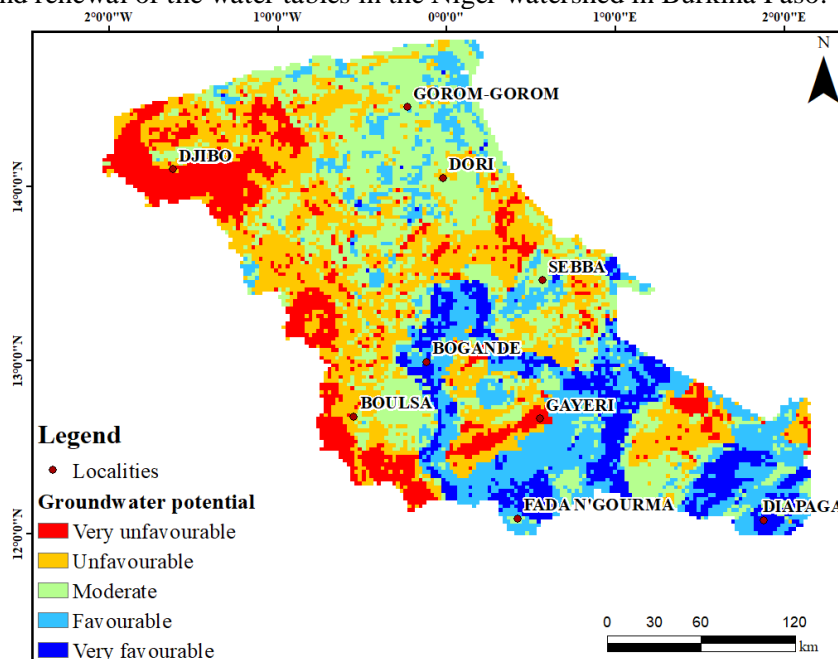


Figure 4: Aquifer potential in the Niger Basin (PAEA, 2022)

5. CONCLUSION

The main objective of this study was to assess the sensitivity of the AHP model in mapping the recharge potential of aquifers. Based on previous work, six criteria governing recharge potential were selected and mapped using existing spatial techniques and databases. The novelty of this study is the incorporation of probabilistic Monte Carlo uncertainty into the AHP method. This made it possible to model expert judgement. This modelling provided an adjustment of the class limits of aquifer recharge potential in order to bring them closer to the reality on the ground. This observation was confirmed by analysis of the ROC and AUC curves, indicating that the MC-AHP model performed better than the AHP model. Overall, this approach has provided valuable information on the recharge potential of aquifers in the Niger basin in Burkina Faso. As a result, we suggest that local and regional water resource administrative authorities prioritize these favorable areas of recharge potential in order to improve the quality and renewal of groundwater in the watershed. In addition, this study reveals that soil types are the most significant criteria governing aquifer recharge in the basement.

This study demonstrates the potential of the SAHP approach for groundwater recharge assessment; however, some limitations remain. The results depend on the quality and resolution of input data, and certain assumptions such as the independence and temporal stability of factors may not fully reflect real conditions. Moreover, limited field validation introduces uncertainty in the suitability map. Future work should integrate dynamic climate and land-use data, apply advanced remote sensing and machine learning techniques, and strengthen field validation to improve the robustness and transferability of the SAHP framework.

Author contributions: Y.K: Conceptualisation, methodology, project administration, supervision, validation, writing, revision. I.K: Research, methodology, software, data curation, visualisation and writing-original version. N.D: Methodology, software, data curation, revision.

Funding: The authors would like to thank the Geosciences and Environment Laboratory (LaGE) for its material support for this research project and for carrying out this study and the Directorate-General for Water Resources (DGRE) for the availability of data on groundwater levels in boreholes.

Acknowledgments: The authors would also like to thank the editors and reviewers. Their comments have greatly improved the manuscript.

Competing interests: The authors declare no conflict of interest.

Data availability: All satellite data sets used in this study come from publicly available data repositories

REFERENCES

- [1] T. Saaty, (1980). *The Analytic Hierarchy Process: Planning, Priority Setting, Resource Allocation*; McGraw-Hill: New York, NY, USA.
- [2] L. Jing, B. Chen, B. Zhang, P. Li, J. Zheng, (2013). Monte Carlo Simulation–Aided Analytic Hierarchy Process Approach: Case Study of Assessing Preferred Non-Point-Source Pollution Control Best Management Practices. *Journal of Environmental Engineering*, 139 (5), 618–626. [https://doi.org/10.1061/\(ASCE\)EE.1943-7870.0000673](https://doi.org/10.1061/(ASCE)EE.1943-7870.0000673).
- [3] I. Ki, H. Chakroun, Y. Koussoubé, and K. Zouari, (2023). Assessment of Aquifer Recharge Potential Using Remote Sensing, GIS and the Analytical Hierarchy Process (AHP) Combined with

- Hydrochemical and Isotope Data (Tamassari Basin, Burkina Faso). *Water*, 15(4), Article 4. <https://doi.org/10.3390/w15040650>.
- [4] S. Oularé, G. C. Adon, L. Y. Akpa, M. B. Saley, F. K. Kouamé, and R. Therrien, (2017). Identification Des Zones Potentielles De Recharge Des Aquifères Fracturés Du Bassin Versant Du N'zo (Ouest De La Côte d'Ivoire): Contribution Du SIG Et De La Télédétection. *European Scientific Journal, ESJ*, 13(36), 192. <https://doi.org/10.19044/esj.2017.v13n36p192>.
- [5] J. Jourda, S. Mahaman Bachir, and E. Djagoua, (2006). Utilisation des données ETM de landsat et d'un SIG pour l'évaluation du potentiel en eau souterraine dans le milieu fissuré précambrien de la région de Korhogo (Nord de la Côte d'Ivoire): Approche par analyse multicritère et test de validation. *Contemporary publishing International*, 5(4), 339-357.
- [6] N. Dahri, and H. Abida, (2017). Monte Carlo simulation-aided analytical hierarchy process (AHP) for flood susceptibility mapping in Gabes Basin (southeastern Tunisia). *Environmental Earth Sciences*, 76(7), 302. <https://doi.org/10.1007/s12665-017-6619-4>.
- [7] G. Coates, and S. Rahimifard, (2009). Modelling of post-fragmentation waste stream processing within UK shredder facilities. *Waste Management*, 29(1), 44-53. <https://doi.org/10.1016/j.wasman.2008.03.006>.
- [8] R. J. Lake, P. J. Cressey, D. M. Campbell, and E. Oakley, (2010). Risk ranking for foodborne microbial hazards in New Zealand: Burden of disease estimates. *Risk Analysis: An Official Publication of the Society for Risk Analysis*, 30(5), 743-752. <https://doi.org/10.1111/j.1539-6924.2009.01269.x>.
- [9] MEA. (2016). Programme National d'Approvisionnement en Eau Potable 2016-2030.
- [10] Banque mondiale. (2017). Mission de pré-identification d'un nouveau Projet Dans le Secteur de l'Eau et de l'Assainissement et atelier de restitution de l'étude de la connaissance et de la gestion des ressources en eau : 26 au 30 juin 2017.
- [11] IWACO. (2001). État des lieux des ressources en eau du Burkina Faso et de leur cadre de gestion. (p.241) [Rapport d'étude].
- [12] C. Castaing, M. Billa, J. P. Milesi, D. Thieblemont, J. Lemetour, F. Egal, M. Donzeau, C. Guerro, A. Cocherie, P. Chevremont, M. Tegye, Y. Itard, B. Zida, I. Ouedraogo, S. Kote, B. E. Kaboré, C. Ouedraogo, J. C. Ki, and C. Zunino, (2003). Notice explicative de la carte géologique et minière à 1/1 000 000ème du Burkina Faso. [Explanatory Note of the 1/1.000.000 Mining and Geological Map of Burkina Faso.] BUMIGEB, Ouagadougou. (In French)—References—Scientific Research Publishing.
- [13] PAEA. (2022). Etude d'identification des zones d'aquifères favorables par l'analyse multicritère, d'implantation des forages productifs en zone de socle et contrôle de réalisation de forages. (p. 224) [Rapport d'étude].
- [14] J. L. Castillo, D. A. Martínez, J. A. Ramos, J. V. Tuxpan, S. T. A. Rodríguez Tapia, and A. C. E. Marín, (2022). Delineation of Groundwater Potential Zones (GWPZs) in a Semi-Arid Basin through Remote Sensing, GIS, and AHP Approaches. *Water*, 14(13), Article 13. <https://doi.org/10.3390/w14132138>.
- [15] O. Ait El Mekki, (2017). Spatialisation du potentiel de recharge diffuse d'un aquifère libre sous climat semi-aride par techniques géospatiales et hydrochimiques: Cas de l'aquifère du Haouz (Marrakech, Maroc) [These de doctorat, Université Cadi Ayyad Faculté Des Sciences Semlalia Marrakech (Maroc)]. <https://theses.hal.science/tel-01725794>.
- [16] M. Youan Ta, T. Lasm, J. P. Jourda, K. F. Kouamé, and M. Razack, (2008). Cartographie des accidents géologiques par imagerie satellitaire Landsat-7 ETM+ et analyse des réseaux de fractures du socle précambrien de la région de Bondoukou (nord-est de la Côte d'Ivoire). *Teledetection*, 8(2), 119.
- [17] Y. N. Akokponhoué, N. Yalo, M. Y. Ta, H. B. Akokponhoué, and G. Agbahoungba, (2019). Apport de la télédétection et de la géophysique dans la cartographie des fractures hydrauliquement actives en zone de socle au Centre-Ouest du Benin. *Eur. Sci. J*, 15, 426-447.
- [18] M. S. Alshayef, A. M. Mohammed, A. Javed, and M. A. Albaroot, (2017). Manual and automatic extraction of lineaments from multispectral image in part of Al-Rawdah, Shabwah, Yemen by using remote sensing and GIS technology. *International Journal of New Technology and Research*, 3(2), 263346.
- [19] M. Koita, (2010). Caractérisation et modélisation du fonctionnement hydrodynamique d'un aquifère fracturé en zone de socle: Région de Dimbokro-Bongouanou (Centre Est de la Côte d'Ivoire).

- [20] F. Bonn, and G. Rochon, (1992). Précis de télédétection volume 1 : Principes et méthodes. Sainte-Foy: Presse de l'université du Québec/AUPELF.
- [21] Z. Adiri, A. El Harti, A. Jellouli, R. Lhissou, L. Maacha, M. Azmi, M. Zouhair, and E. M. Bachaoui, (2017). Comparison of Landsat-8, ASTER and Sentinel 1 satellite remote sensing data in automatic lineaments extraction : A case study of Sidi Flah-Bouskour inlier, Moroccan Anti Atlas. *Advances in Space Research*, 60(11), 2355-2367. <https://doi.org/10.1016/j.asr.2017.09.006>.
- [22] GeoBretagne. (2022). Comprendre une image satellitaire—Rayonnement. GeoBretagne. <https://cms.geobretagne.fr/>.
- [23] H. F. Yeh, Y. S. Cheng, H. I. Lin, and C. H. Lee, (2016). Mapping groundwater recharge potential zone using a GIS approach in Hualian River, Taiwan. *Sustainable Environment Research*, 26(1), Article 1. <https://doi.org/10.1016/j.serj.2015.09.005>.
- [24] G. E. Ake, K. J. Kouame, A. B. Koffi, and J. P. Jourda, (2018). Cartographie des zones potentielles de recharge de la nappe de Bonoua (sud-est de la Côte d'Ivoire). *Revue des sciences de l'eau*, 31(2), 129-144. <https://doi.org/10.7202/1051696ar>.
- [25] D. Diriba, S. Karuppanan, T. Takele, and M. Husein, (2024). Delineation of groundwater potential zonation using geoinformatics and AHP techniques with remote sensing data. *Heliyon*, 10(3). <https://doi.org/10.1016/j.heliyon.2024.e25532>.
- [26] M. B. Saley, (2003). Système d'informations hydrogéologiques à référence spatiale, discontinuités pseudo-images et cartographies thématiques des ressources en eau de la région semi-montagneuse de Man (Ouest de la Côte d'Ivoire). Abidjan, Côte d'Ivoire: Thèse de Doctorat de l'Université de Cocody.
- [27] W. Fazar, (1959). Program evaluation and review technique. *The American Statistician*, 13(2), 646-669.
- [28] H. Chakroun, (2018). Atelier : Spatial Decision Support System (SDSS) in QGIS.
- [29] B. Chen, L. Jing, J. Zheng, and P. Li, (2011). Integrated management of nonpoint source pollution in the City of Chongzhou, China. In *Technical Rep : Prepared for the Water Governance Program of United Nations Development Program (UNDP)*. [Technical Rep].
- [30] A. Hébie, (2019). Fonctionnement hydrogéologique des nappes d'eau souterraine sur le territoire communal de Ouahigouya. Approche de la recharge des nappes par un suivi piézométrique [Mémoire de masters]. Université Joseph KI-ZERBO.
- [31] A. M. S. Babaye, (2012). Evaluation des ressources en eau souterraine dans le bassin de Dargol (Liptako Niger) [These de doctorat, Université de Liège]. <https://scholar.archive.org/work/xe5yg2ck2fe75bxgtcailor6j4>.
- [32] Y. Koussoubé, (2010). Hydrogéologie des séries sédimentaires de la dépression piézométrique du Gondo (bassin du Sourou) : Burkina Faso / Mali [These de doctorat]. Université Pierre et Marie Curie - Paris VI.
- [33] G. Favreau, (2000). Caractérisation et modélisation d'une nappe phréatique en hausse au Sahel : Dynamique et géochimie de la dépression piézométrique naturelle du kori de Dantiandou (sud-ouest du Niger) [These de doctorat]. Université Paris Sud XI.
- [34] C. Leduc, and F. Lenoir, (1995). Etude de la Recharge du Nappe du Terminal Continental 3 dans le Fleuve Gauche du Niger. In : Lebel T (ed.). *Hydrologie et météorologie de méso-échelle dans HAPEX-Sahel : Dispositif de mesures au sol et premiers résultats*. ORSTOM.
- [35] M. S. Kutangila, (2019). Caractérisation hydrogéologique des aquifères du bassin sédimentaire de Taoudéni (bordure sud-est, Burkina Faso)—Sécheresse info [Mémoire de masters]. Institut International d'Ingénierie de l'eau de l'Environnement.
- [36] Y. Tamesgen, A. Atlabachew, and M. Jothimani, (2023). Groundwater potential assessment in the Blue Nile River catchment, Ethiopia, using geospatial and multi-criteria decision-making techniques. *Heliyon*, 9(6). <https://doi.org/10.1016/j.heliyon.2023.e17616>.
- [37] S. A. Naghibi, and M. M. Dashtpajardi, (2017). Evaluation of four supervised learning methods for groundwater spring potential mapping in Khalkhal region (Iran) using GIS-based features. *Hydrogeology journal*, 25(1), 169.
- [38] B.-H. Nam, and R. B. D'Agostino, (2002). Discrimination Index, the Area Under the ROC Curve. In C. Huber-Carol, N. Balakrishnan, M. S. Nikulin, & M. Mesbah (Éds.), *Goodness-of-Fit Tests and Model Validity* (p. 267-279). Birkhäuser. https://doi.org/10.1007/978-1-4612-0103-8_20.
- [39] S. Miraki, S. H. Zanganeh, K. Chapi, V. P. Singh, A. Shirzadi, H. Shahabi, and B. T. Pham, (2019). Mapping Groundwater Potential Using a Novel Hybrid Intelligence Approach. *Water Resources Management*, 33(1), 281-302. <https://doi.org/10.1007/s11269-018-2102-6>.

- [40] E. Yesilnacar, and T. Topal, (2005). Landslide susceptibility mapping : A comparison of logistic regression and neural networks methods in a medium scale study, Hendek region (Turkey). *Engineering Geology*, 79(3), 251-266. <https://doi.org/10.1016/j.enggeo.2005.02.002>.
- [41] S. Boulahbal, (2012). Etude des écoulements souterrains dans les gneiss schisteux fissurés du Précambrien de la région de Tamanrasset [Magister, Université de Batna 2]. <http://eprints.univbatna2.dz/833/>.
- [42] K. F. Kouamé, (1999). Hydrogéologie des aquifères discontinus de la région semi-montagneuse de Man-Danané Ouest de la Côte d'Ivoire). Apport des données des images satellitales et des méthodes statistique et fractale à l'élaboration d'un système d'information hydrogéologique à référence spatiale [These de doctorat]. Université de Cocody.
- [43] J. P. Laborde, (2009). Elément d'hydrologie de surface.
- [44] F. Rioult, (2011). Interprétation graphique de la courbe ROC. Extraction et Gestion des Connaissances (EGC'11), 6 p. <https://hal.science/hal-01018456>.